NASA TECHNICAL NOTE

NASA TN D-5652

NASA TN D-5652

SURVEY OF LITERATURE ON FLOW CHARACTERISTICS OF A SINGLE TURBULENT JET IMPINGING ON A FLAT PLATE

by James W. Gauntner, John N. B. Livingood, and Peter Hrycak

Lewis Research Center
Cleveland, Ohio

NATIONAL AERONAUTICS AND SPACE ADMINISTRATION • WASHINGTON, D. C. • FEBRUARY 1970

1. Report No. NASA TN D-5652	2. Government Accession No.	3. Recipient's Catalog No.
4. Title and Subtitle SURVEY OF LITERATURE ON FLOW CHARACTERISTICS OF A SINGLE TURBULENT JET IMPINGING ON A FLAT PLATE		5. Report Date February 1970
		6. Performing Organization Code
7. Author(s) James W. Gauntner and John N. B. Livingood, Lewis Research Center; and Peter Hrycak, Newark College of Engineering		8. Performing Organization Report No. E-5203
9. Performing Organization Name and Address Lewis Research Center National Aeronautics and Space Administration Cleveland, Ohio 44135		10. Work Unit No. 720-03
		11. Contract or Grant No.
		13. Type of Report and Period Covered Technical Note
12. Sponsoring Agency Name and Address National Aeronautics and Space Administration Washington, D.C. 20546		
		14. Sponsoring Agency Code

15. Supplementary Notes

16. Abstract

Flow characteristics of single jets impinging on flat surfaces have been studied by many investigators. The results of some of the numerous studies are summarized herein. Suggested methods for determining velocities and pressures on which to base heat-transfer correlations for use in impingement cooling design are presented.

17. Key Words (Suggested by Author(s)) Literature survey Impinging jet Flat plate Flow characteristics	18. Distribution Statement Unclassified - unlimited		
19. Security Classif. (of this report) Unclassified	20. Security Classif. (of this page) Unclassified	21. No. of Pages 45	22. Price* $3.00

*For sale by the Clearinghouse for Federal Scientific and Technical Information
Springfield, Virginia 22151

CONTENTS

SURVEY OF LITERATURE ON FLOW CHARACTERISTICS OF A SINGLE

TURBULENT JET IMPINGING ON A FLAT PLATE

by James W. Gauntner, John N. B. Livingood, and Peter Hrycak*

Lewis Research Center

SUMMARY

The results of an extensive survey of the flow characteristics of a single jet imping-
ing on a flat surface are presented herein. The flow field consists of four distinct re-
gions, each of which is discussed in detail. Methods for predicting the spread of the jet,
and velocity and pressure profiles in the various regions, are presented.

Comparisons between theory and experimental data are presented for velocity dis-
tributions in the various flow regions. Experimental data for velocity fluctuations due to
turbulence are also shown. Some suggested velocities on which to base heat-transfer
correlations for use in impingement cooling design and some areas requiring further
investigations are also discussed.

INTRODUCTION

A promising method for cooling turbine vanes or blades is to impinge cool air on
the internal surfaces of the vanes or blades. Although numerous investigators have
studied the impingement of air jets on flat plates, heat-transfer results differ so widely
that no adequate heat-transfer correlation for design use is available. It is for this
reason that the NASA Lewis Research Center initiated an impingement cooling program.
The ultimate goals of this program are to develop design heat-transfer correlations to
apply to cylindrically shaped leading edges of vanes or blades and for impingement cool-
ing along the vane or blade suction and pressure surfaces. The initial phase is limited
to impingement on a flat plate. Such results may be applicable for cooling blade suction
and pressure surfaces.

Development of adequate heat-transfer correlations depends on a knowledge of flow
characteristics. A number of investigators have studied the flow phenomena of free jets

---

*Professor of Mechanical Engineering, Newark College of Engineering, Newark, N.J.

issuing from both circular holes and slots. Some have also investigated jets impinging on flat surfaces. Our purpose herein is to summarize many of these previous studies and to include derivations of useful equations for determining pressures and velocities in the flow field. This report is based, in part, on a survey of literature on flow and heat transfer caused by impingement on a flat plate completed under NASA Grant NGR 31-009-004 by Professor Peter Hrycak of the Newark College of Engineering. This report is restricted to the study of the flow field of a single jet impinging on a smooth flat plate.

DESCRIPTION OF FLOW REGIONS

The various flow regions formed by a jet impinging on a solid surface have been discussed by previous investigators (e.g., refs. 1 and 2). In the case of an impinging jet, four distinct flow regions can be characterized. These are shown in figure 1 (symbols defined in the appendix) and are described as follows:

(1) Region I is the region of flow establishment. It extends from the nozzle exit to the apex of the potential core. The so-called potential core is the central portion of the flow in which the velocity remains constant and equal to the velocity at the nozzle exit.
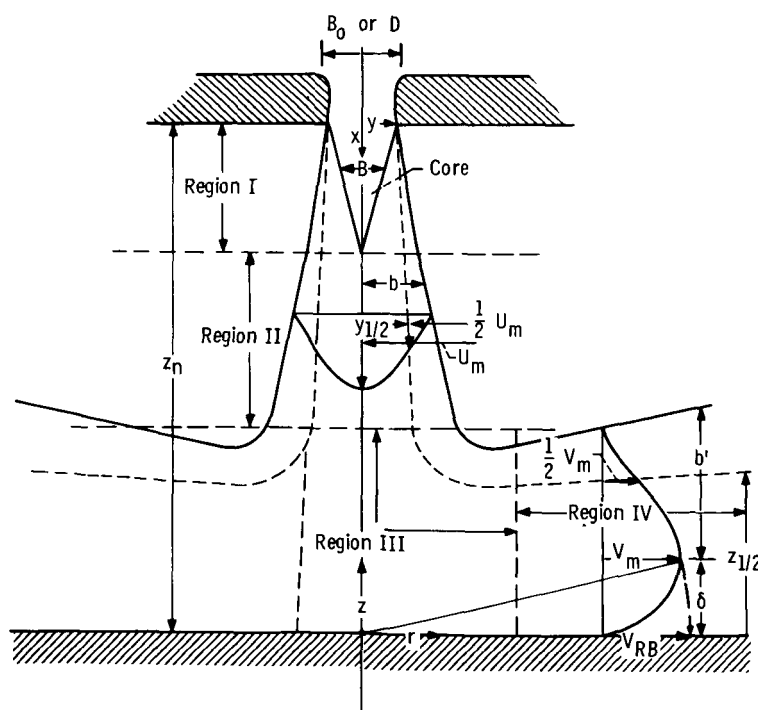

Figure 1. - Characteristic regions in impinging jet flow.

(2) Region II is a region of established flow in the direction of the jet beyond the apex of the potential core; it is characterized by a dissipation of the centerline jet velocity and by a spreading of the jet in the transverse direction.

(3) Region III is that region in which the jet is deflected from the axial direction.

(4) Region IV is known as the wall jet region, where the directed flow increases in thickness as the boundary layer builds up along the solid surface.

GENERAL FEATURES OF JETS

Of fundamental importance in the study of impinging jets (or any jet) is the distinction between laminar and turbulent jets. Reference 3 states that the critical Reynolds number Re_0 (based on nozzle diameter and nozzle exit velocity) which distinguishes laminar jets from turbulent jets is about 1000. Reference 4 reports four characteristic jet patterns for free jets, namely,

(1) The dissipated laminar jet, $Re_0 < 300$. In this case, the viscous forces are large compared to the inertial forces, and the jet diffuses rapidly into the surrounding fluid.

(2) Fully laminar jets, $300 < Re_0 < 1000$. In this case, there is no noticeable diffusion of the jet into the surrounding fluid.

(3) A transition or semiturbulent jet, $1000 < Re_0 < 3000$.

(4) A fully turbulent jet, $Re_0 > 3000$.

These results are confirmed in reference 5, which also states that jets are turbulent for $Re_0 > 3000$. Reference 6, however, refers to a turbulent jet as having Re_0 greater than 14 000. The reason for this difference in Re_0 at which turbulence begins could not be resolved from information contained in the references. The fact that differences have been obtained indicates that further work is required to determine the factors affecting this characteristic. From a heat-transfer standpoint, the determination of Re_0 at which a jet becomes turbulent is vital because applications of cooling with impinging jets involve Re_0 as low as 3000.

With regard to different regions of the jet, reference 7 states that two different modes of heat transfer exist. The first mode applies to the potential core region, where turbulent fluctuations cause the variation in the heat-transfer coefficient. The second mode is for the region of established flow, where both turbulence and velocity cause the variation.

The preceding discussion relating jet pattern to Re_0 range dealt only with jets issuing from circular openings. However, it appears to apply also to jets issuing from slots. Reference 8 indicates that slot jets are turbulent for $Re_0 = 2000$ (here Re_0 is based on the slot width, whereas for circular jets it is based on jet diameter).

The disturbance created by a solid wall on an impinging jet is propagated upstream at a rate equal to the difference between the sonic velocity and the fluid velocity. The wall effect would therefore diminish with increasing Mach number and would finally disappear when the Mach number equaled 1 and the disturbance created by the wall would be unable to propagate upstream.

In a theoretical study reported by Levey (ref. 9) the effect of the impingement surface on the jet was not felt by the jet as close as only 1 slot width away from the surface; this study was for an idealized case (incompressible flow) with no account for viscous effects or turbulent mixing. An experimental study reported in reference 10 confirms the theoretical results; no surface effect on the jet was observed beyond about 2 jet diameters from the plate. Consequently, an impinging jet can be considered to behave like a free jet except in the immediate vicinity of the impingement surface.

REGION OF FLOW ESTABLISHMENT (REGION I)

Near the nozzle opening, a mixing zone originates and turbulent exchange of heat and mass takes place. The mixing zone grows in width in the downstream direction of the jet, leaving a potential core wherein fluid properties and velocity are relatively constant. Eventually, the core is dissipated as a result of the mixing action.

According to Schlichting (ref. 11), by a judicious selection of the origin in the coordinate system, the half width b (see fig. 1) of the free jet is directly proportional to the distance along the jet centerline; that is,

$$b = \text{Constant } x \tag{1}$$

This equation may be used as an approximation for the underdeveloped jet. According to reference 12, the pressure in region I is virtually constant and equal to the pressure in the surrounding fluid. Hence, the total momentum per unit time should be the same for all cross sections normal to the jet; that is,

$$J = \int U \, dM = \rho \int_0^\infty U^2 \, dA = \text{Constant} \tag{2}$$

Velocity Profile

Experimental data of reference 13 suggest that the sole force producing the deceleration of the jet and the acceleration of the surrounding fluid is the tangential shear within the mixing region. An approximate analysis of the mean velocity distribution was presented in reference 13 and is summarized in this section (see fig. 2).
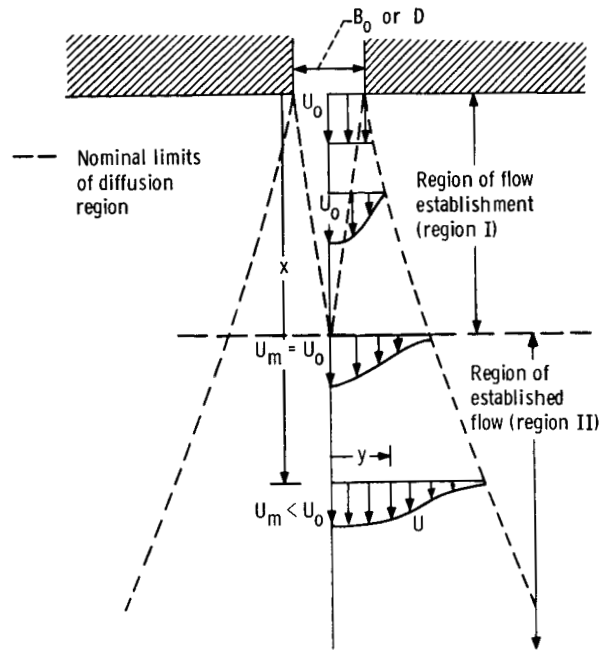
Figure 2. - Schematic representation of jet diffusion.

The volumetric flow rate Q past successive normal sections may be written as

$$Q = \int_0^\infty U \, dA \tag{3}$$

Since Q varies with longitudinal distance x, its ratio to Q_0 (at nozzle exit) is

$$\frac{Q}{Q_0} = \frac{\int_0^\infty U \, dA}{U_0 A_0} \tag{4}$$

where A_0 is nozzle exit area. Also, since momentum flux J may be expressed as the integral of the volume rate of flow $U \, dA$ times the longitudinal component of momentum per unit volume ρU,

$$\frac{J}{J_o} = \frac{\int_0^\infty U^2 \, dA}{U_o^2 A_o} \tag{5}$$

Also, energy flux equals the integral of the local volume flux $U \, dA$ times the kinetic energy per unit volume $\rho(U^2/2)$,

$$\frac{E}{E_o} = \frac{\int_0^\infty U^3 \, dA}{U_o^3 A_o} \tag{6}$$

Since the tangential shear within the mixing zone causes the deceleration of the jet and the acceleration of the surrounding fluid and since this is an internal process, the momentum flux must be constant at every normal section; that is,

$$\frac{J}{J_o} = \frac{\int_0^\infty U^2 \, dA}{U_o^2 A_o} = 1 \tag{7}$$

If viscous action has no influence on the mixing process, the mean flow should be dynamically similar under all conditions. Thus, a similar velocity profile must characterize every section in the diffusion region. As a matter of fact, experimental data follow the general trend of the Gaussian distribution

$$\frac{U}{U_m} = \exp\left(-\frac{y^2}{2\sigma^2}\right) \tag{8}$$

where y is the transverse distance from the jet centerline or axis and σ is the standard or root-mean-square deviation (the value of y for which $U = 0.606 \, U_m$; see fig. 3). This equation is merely a result of a curve fit and has no theoretical basis. The condition of dynamic similarity requires that at all cross sections, regardless of the efflux velocity,

$$\frac{\sigma}{x} = K_1 \tag{9}$$

$$U = 0.606 \, U_m$$

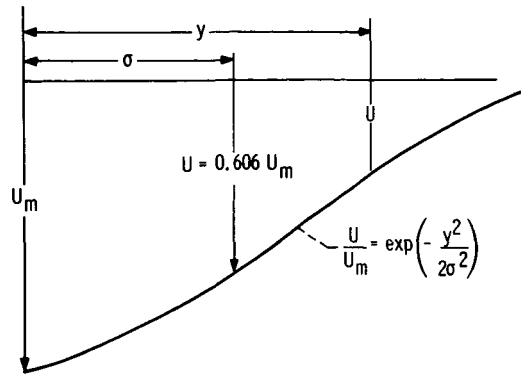$$\frac{U}{U_m} = \exp\left(-\frac{y^2}{2\sigma^2}\right)$$

Figure 3. - Characteristics of normal probability curve.

for the slot jet and

$$\frac{\sigma}{x} = K_2 \tag{10}$$

for the circular jet (i. e., the angle of jet diffusion is a constant). Values of K_1 and K_2 must be determined experimentally. In real jets, the angle of jet diffusion is not necessarily a constant immediately downstream from the nozzle. In reference 13, σ/x proves to be different for both the developed jet (region II) and the developing jet (region I). Still an attempt has been made in reference 13 to treat the jet as if the same experimental constant were applicable for both regions.

Using equations (8) and (10) in evaluating equation (7) yields an expression relating the average nozzle exit velocity to the axial velocity at any point downstream of the potential core for the circular jet

$$\frac{J}{J_o} = \frac{U_m^2 K_2^2 x^2 \pi}{U_o^2 A_o} = 1 \tag{11}$$

This equation can then be evaluated at the point where the potential core region ends (i. e., where x equals x_c and U_m still equals U_o). The appropriate value of A_o may also be substituted into equation (11). Similar substitutions can be made for the slot jet, where the momentum is put on a per unit length basis. These substitutions yield

$$\frac{x_c}{B_o} = \frac{1}{\sqrt{\pi} K_1} \tag{12}$$

for the two dimensional jet and

$$\frac{x_c}{D} = \frac{1}{2K_2}$$ (13)

for the circular jet. The nominal inner boundary of the diffusion region satisfies the equation

$$\left.\begin{array}{l} \dfrac{B}{B_o} = 1 - \dfrac{\sqrt{\pi}\,K_1 x}{B_o} \\[4ex] \dfrac{B}{D} = 1 - \dfrac{2K_2 x}{D} \end{array}\right\}$$ (14)

or

where B is the width of the potential core at a distance x from the nozzle. The velocity distribution in the diffusion zone of region I, obtained by combining equations (8) to (10) and (14), becomes

$$\frac{U}{U_o} = \exp\left[-\frac{\left(y + \dfrac{\sqrt{\pi}\,K_1 x}{2} - \dfrac{B_o}{2}\right)^2}{2(K_1 x)^2}\right]$$ (15)

for a slot of half width $B_o/2$ and

$$\frac{U}{U_o} = \exp\left[-\frac{\left(y + K_2 x - \dfrac{D}{2}\right)^2}{2(K_2 x)^2}\right]$$ (16)

for a circular jet. Experimental data are compared in figures 10 and 16 of reference 13 with results calculated from equations (15) and (16), respectively. Satisfactory agreement between equation (15) and experiment is shown in figure 10 of reference 13. Experimental data shown in figure 16 of reference 13 deviate considerably from equation (16). This is due to the fact that reference 13 attempted to use a single value of σ/x for both the region of flow establishment and the region of established flow. A better comparison would result by using the value of σ/x associated with region I.

8

Potential Core Length

It was previously stated that region I extends from the nozzle to the apex of the potential core. The potential core length considered in this report is sometimes called the nominal potential core length and its determination requires a knowledge of the centerline velocity decay in region II. For that reason, some material which in reality belongs in region II is presented under region I and then not repeated in region II. The actual potential core length, which corresponds to the spacing between the virtual origin of the jet and the point where the jet centerline velocity begins to decrease, is not referred to herein. If equation (11) is solved for the ratio of the centerline velocity to the average nozzle velocity for the circular jet, and a similar equation is solved for the slot jet, the following expressions result:

$$\frac{U_m}{U_o} = \frac{\sqrt{\dfrac{1}{\sqrt{\pi}K_1}}}{\sqrt{\dfrac{x}{B_o}}} \tag{17}$$

for the slot jet and

$$\frac{U_m}{U_o} = \frac{\dfrac{1}{2K_2}}{\dfrac{x}{D}} \tag{18}$$

for the circular jet. These equations may be reexpressed, using equations (12) and (13), as

$$\frac{U_m}{U_o} = \frac{\sqrt{\dfrac{x_c}{B_o}}}{\sqrt{\dfrac{x}{B_o}}} = \frac{\sqrt{C_1}}{\sqrt{\dfrac{x}{B_o}}} \tag{17}$$

$$\frac{U_m}{U_o} = \frac{\dfrac{x_c}{D}}{\dfrac{x}{D}} = \frac{C_2}{\dfrac{x}{D}} \tag{18}$$

The nondimensional potential core lengths C_1 and C_2 in equations (17) and (18) are for the slot jet and the circular jet, respectively.

Although equations (17) and (18) are only valid beyond the potential core (region I), they may be used to experimentally determine the length of the potential core in the following way. Log-log plots of the measured centerline velocity ratio U_m/U_o against x/B_o (or x/D) yield lines with slopes $-1/2$ or -1, respectively, for the slot jet and the circular jet. Extension of these lines to intersect $U_m/U_o = 1$ then gives the desired length of the potential core, C_1 for the slot jet or C_2 for the circular jet.

Schlichting (ref. 11) presents the following equation for the velocity distribution in the axial direction of a developed laminar circular jet, from which an analytical expression for the nominal potential core length can be obtained:

$$U = \frac{3}{8\pi} \frac{K}{\nu x} \frac{1}{\left(1 + \dfrac{1}{4}\xi^2\right)^2} \tag{19}$$

where the kinematic momentum flux

$$K = 2\pi \int_0^\infty U^2 y \, dy$$

and

$$\xi = \sqrt{\frac{3K}{16\pi}} \frac{y}{\nu x} \tag{20}$$

Along the jet axis, $\xi = 0$ and the velocity distribution along the axis reduces to

$$U_m = \frac{3}{8\pi} \frac{K}{\nu x} \tag{21}$$

and

10

$$K = \frac{\pi U_o^2 D^2}{4} \tag{22}$$

Therefore,

$$U_m = \frac{3}{8\pi} \frac{1}{\nu x} \frac{\pi U_o^2 D^2}{4}$$

or

$$\frac{U_m}{U_o} = \frac{3}{32} Re_o \left(\frac{x}{D}\right)^{-1} \tag{23}$$

This last equation is similar to equation (18) and shows that the potential core length for laminar flow (the coefficient of $(x/D)^{-1}$, which in this case is $(3/32)Re_o$) is a function of the nozzle Reynolds number.

For turbulent flow, the axial velocity is represented by equation (19) if, according to reference 11 the laminar flow kinematic viscosity ν is replaced by the virtual kinematic viscosity ϵ for turbulent flow, where ϵ has been evaluated as

$$\epsilon = 0.0256 \, Uy_{1/2} \tag{24}$$

It is shown that $y \propto x$ and $U \propto x^{-1}$ (for similar flow). Hence, it is possible to express ϵ as

$$\epsilon = \nu\gamma Re_o \tag{25}$$

where γ is a proportionality factor. The resulting equation for the jet centerline axial velocity for the turbulent flow case then becomes

or

$$\left. \begin{aligned} U_m &= \frac{3}{32} \frac{U_o^2 D^2}{\gamma \nu Re_o x} \\[2em] \frac{U_m}{U_o} &= \frac{3}{32\gamma} \left(\frac{x}{D}\right)^{-1} \end{aligned} \right\} \tag{26}$$

Hence, for turbulent flow, the length of the potential core is $(3/32)\gamma$ and is independent of the nozzle Reynolds number as long as flow remains similar and the definition of ϵ holds.

Another expression for potential core length of a turbulent circular jet may be obtained from the results of Tollmien. He analyzed the flow in the downstream part of a turbulent submerged axially symmetric jet. His solution may be used to get the expression shown in reference 12

$$\frac{U_m}{U_o} = \frac{0.48\ D}{ax} \tag{27}$$

This result was obtained with the use of a similarity variable

$$\varphi = \frac{y}{ax} \tag{28}$$

and numerical integration. From table I in reference 14, when $U = U_m/2$ and $y = y_{1/2}$, $\varphi = 1.23$. From experiments described in reference 12,

$$y_{1/2} = 0.097\ x \tag{29}$$

Hence, from equations (27) to (29),

$$\frac{U_m}{U_o} = \frac{0.48D\varphi}{y_{1/2}} \simeq 6.1\frac{D}{x} \tag{30}$$

Comparison of this result with equation (18) shows $C_2 \simeq 6.1$ for a circular jet.

Unfortunately, values of core lengths differ for investigations carried out by different experimenters. The amount of divergence which different observers report generally exceeds the expected experimental error and is more than likely explained by the effect of the scale and the intensity of turbulence within the jet. Also the actual velocity distribution at the nozzle seems to be a factor. The following two paragraphs give the results of some of the previous investigators and some information concerning their experiments.

For slot jets, Albertson (ref. 13) states that the potential core extends 5.2 slot widths. He investigated air flowing through slots of widths 1/4, 1/16, and 1/32 inch (0.635, 0.159, and 0.079 cm) for a range of Reynolds numbers

12

$$1.5 \times 10^3 < Re_o < 7.2 \times 10^4$$

Schauer and Eustis (ref. 15) investigated a 1/2-inch (1.27-cm) slot; air impinged on a plate located from 10 to 40 slot widths from the nozzle. The values of Re_o ranged from 2×10^4 to 5.3×10^4. The core length of about 5.5 slot widths used in the analysis presented in reference 15 was obtained by averaging two similar values obtained from the data of van der Hegge Zijnen (ref. 16). Reference 16 considered slot widths of about 0.197 and 0.394 inch (0.5 and 1.0 cm) and a value of Re_o of about 1.3×10^4. Reference 17 reports results for various-sized rectangular, square, elliptical, and triangular slots, for $3.6 \times 10^3 < Re_o < 8.8 \times 10^4$ and arrived at an average value of potential core length of about 7 slot widths.

For circular air jets, reference 13 reported a value for C_2 of 6.2 after testing nozzles 1/4, 1/2, and 1 inch (0.635, 1.27, and 2.54 cm) in diameter for values of Re_o from 2.2×10^4 to 8.7×10^4. Pai (ref. 18) reported a value for C_2 of 6.5. From the results of Tani and Komatsu (ref. 10), the corresponding value for C_2 is about 4.8; this result was obtained from data for air flowing through nozzles with diameters of about 2.05 and 3.27 inches (5.2 and 8.3 cm) and impinging on a plate 2 to 15 diameters from the nozzle. Poreh and Cermak (ref. 1) experimented with water flowing through nozzles 3/4, 1, and $1\frac{1}{2}$ inches (1.905, 2.54, and 3.81 cm) in diameter impinging on a plate located from 8 to 32 nozzle diameters from the nozzle; they report a value for C_2 of 7.7. From data shown on figure 2 of reference 1, the local jet centerline velocity can be observed to be about 10 percent higher than the average nozzle exit velocity. If the potential core length of reference 1 were to be reexpressed in terms of the maximum nozzle exit velocity, the numerical value would be more comparable to values obtained by other investigators.

In an appendix to reference 13, Baines examined the results of Albertson more closely and concluded that the Reynolds number has an effect on the potential core length. He recommended values for C_2 of 5 for $Re_o = 1.4 \times 10^4$ and 7 for $Re_o = 10^5$. Abramovich (ref. 12), however, asserts that the value of C_2 does not vary with Reynolds number but does vary with the velocity profile. However, since the velocity profile in turbulent flow may be considered to be a weak function of the Reynolds number, to some extent C_2 could vary with Re_o as Baines suggested. However, theory based on Prandtl's second hypothesis shows that, for developed turbulent flow, the potential core length is independent of the Reynolds number (eq. (26)).

To summarize, it has been noted that, for turbulent flow, potential core lengths varying from about 4.7 to 7.7 have been obtained by different investigators. Moreover, some investigators state that core length is dependent on Re_o, while others state that core length is independent of Re_o. This latter view is supported by equation (26) of this re-

port. Since, from a heat-transfer standpoint core length is important, it appears that additional work in this area is required.

Centerline Turbulence Distribution

Investigations have shown (refs. 6 and 7) that the local heat-transfer coefficient at the stagnation point on the impingement plate reaches a maximum value at the apex of the potential core. Since the centerline velocity is constant in the potential core, the observed increase in heat-transfer coefficient must be due to the effects of turbulence. Reference 19 shows that the turbulence level on the jet centerline begins to rise at an axial distance of only 1 diameter from the nozzle mouth; this is shown in figure 4, taken from reference 19, for both a 1-inch (2.54-cm) and a 3-inch (7.62-cm) heated circular jet. Nozzle size was also shown to affect turbulence and heat transfer. Consequently, any reference velocities that may be used or applied in heat-transfer analysis or correlation may need to be modified to include the effects of turbulence.
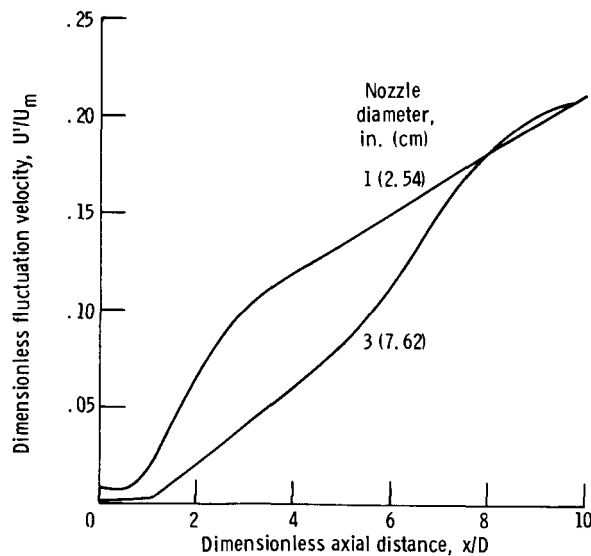
Figure 4. - Turbulence distribution along jet centerline.
(Data from ref. 19.)

Pressure Distribution

The study of turbulent free jets by use of the boundary-layer theory assumes negligible pressure variation in the flow direction. However, reference 20 reports observation of a radial pressure gradient at a value of $x/B_o = 2$ (within the potential core) with the maximum pressure at the centerline higher than ambient. A minimum pressure lower than ambient was observed away from the centerline of the jet. Reference 20 also reports a static pressure ridge, higher than ambient and decaying rapidly with x, in the potential core. The ridge is attributed to the persistence of the pressure distribution created within the nozzle. Outside the core in region I, all measured static pressures were below the ambient pressure.

From available theory and data, it appears that the effect of a pressure gradient in the potential core zone is relatively unimportant with respect to flow development, but it seems to warrant an additional experimental investigation.

Secondary Effects

The preceding discussions were limited to a study of the length of the potential core and the variation of velocity and pressure in the diffusion region. Secondary effects produced by the impingement surface may also have some effect on the jet. These secondary effects are (1) a dynamic instability effect, and (2) a blockage or interference effect. The former is characterized by a lateral oscillation of the complete jet flow field while the latter is distinguished by changes in core length and jet spreading rate.

REGION OF ESTABLISHED FLOW (REGION II)

Some of the analyses that were required to determine the potential core length and the velocity profiles for region I are only applicable to region II. These analyses are not repeated, but reference to the appropriate equations is made.

Centerline Velocity Decay

Based on discussion contained in reference 13, the centerline velocity decay for the slot jet is given by equation (17)

$$\frac{U_m}{U_o} = \sqrt{C_1} \left(\frac{x}{B_o}\right)^{-1/2} \tag{17}$$

and for the circular jet by equation (18)

$$\frac{U_m}{U_o} = C_2 \left(\frac{x}{D}\right)^{-1} \tag{18}$$

Many experimenters (e.g., Albertson et al. (ref. 13)) have investigated the centerline velocity decay, and their results have verified the general form of these equations.

Velocity Profile

According to Schlichting (ref. 11), problems in free turbulent flow are of a boundary-layer nature and can be studied with the aid of equations of boundary-layer type. For the two-dimensional, steady-state case, these equations are

$$U \frac{\partial U}{\partial x} + V \frac{\partial U}{\partial y} = \frac{1}{\rho} \frac{\partial \tau}{\partial y} \tag{31}$$

$$\frac{\partial U}{\partial x} + \frac{\partial V}{\partial y} = 0 \tag{32}$$

where τ denotes the turbulent shearing stress and where the pressure term has been dropped (to a first approximation, the pressure is assumed to be constant).

To obtain the velocity distribution from these equations, it is necessary to express τ in terms of parameters of the main flow. This may be done in three ways:

(1) Use of Prandtl's mixing length theory, where

$$\tau = -\rho \overline{uv} = \rho l^2 \left| \frac{\partial U}{\partial y} \right| \frac{\partial U}{\partial y} \tag{33}$$

(2) Extension of the mixing length theory, where

$$\tau = \rho l^2 \frac{\partial U}{\partial y} \sqrt{\left(\frac{\partial U}{\partial y}\right)^2 + l_1^2 \left(\frac{\partial^2 U}{\partial y^2}\right)^2} \qquad (34)$$

and l and l_1 are to be regarded as purely local functions

(3) Prandtl's second hypothesis

$$\tau = \rho \epsilon \frac{\partial U}{\partial y} = \rho \chi_1 b \left(U_{max} - U_{min}\right) \frac{\partial U}{\partial y} \qquad (35)$$

where b is the half width of the mixing zone (from centerline to outer jet boundary) and χ_1 is an empirical constant. From this, $\epsilon = \chi_1 b \left(U_{max} - U_{min}\right)$ is the virtual kinematic viscosity, assumed to be constant over the whole width and previously used in equation (24).

Tollmien (ref. 14) obtained the velocity distribution by solving the system of equations (31) to (33); the use of equation (33) involves the application of Prandtl's mixing length theory for evaluating the shear stress.

Görtler (ref. 21) solved the system of equations (31), (32), and (35); this solution involved the use of Prandtl's second hypothesis and, according to reference 11, results in a simpler solution. Reference 11 further states that best agreement with experiment is obtained when Görtler's analysis is considered.

Tollmien's solution requires the use of successive approximations. For this reason, and because of the preceding statement, this solution is not reproduced herein. Refer to reference 14 for details of the solution for the two-dimensional and circular jets.

In reference 14, values of U/U_m are tabulated as a function of $y\big/\left(x \sqrt[3]{c^2}\right)$, where $\sqrt[3]{c^2}$ is evaluated as 0.063 and c is the scaling factor in Prandtl's mixing length theory. Instead of using $y\big/\left(x \sqrt[3]{c^2}\right)$ as the abscissa, it is common practice to plot U/U_m against $y/y_{1/2}$, where $y_{1/2}$ is that value of y for which the velocity is equal to $U_m/2$. Hence, when $U/U_m = 0.5$, $y/y_{1/2} = 1$. For the circular jet, a plot of Tollmien's tabulated data shows $U/U_m = 0.5$ when $y\big/\left(x \sqrt[3]{c^2}\right) = 1.23$; hence, if each abscissa is divided by 1.23, values of $y/y_{1/2}$ are obtained, and the ordinates can then be plotted against these new abscissas. The same procedure was used to replot the slot jet solution. This is the way Tollmien's solutions are plotted in this report.

For the two-dimensional jet, according to Schlichting, Görtler's solution may be written as

$$U = \frac{\sqrt{3}}{2} \sqrt{\frac{K\lambda}{x}} \left(1 - \tanh^2 \eta_1\right) \tag{36}$$

$$V = \frac{\sqrt{3}}{4} \sqrt{\frac{K}{\lambda x}} \left[2\eta_1 \left(1 - \tanh^2 \eta_1\right) - \tanh \eta_1\right] \tag{37}$$

where the constant kinematic momentum flux $K = J/\rho$ and

$$\lambda = \frac{1}{2} \sqrt{\frac{U_{m,s} s}{\epsilon_s}} \tag{38}$$

where s is the fixed distance from the nozzle, $U_{m,s}$ is the centerline velocity at s,

$$\epsilon_s = \chi_1 b_s U_{m,s}$$

and

$$\eta_1 = \frac{\lambda y}{x}$$

For this case, λ is the empirical constant. Its value was obtained as 7.67 by Reichardt (ref. 22).

For the circular jet, Görtler's solution is

$$U = \frac{3}{8\pi} \frac{K}{\epsilon x} \frac{1}{\left(1 + \frac{1}{4} \eta_2^2\right)^2} \tag{39}$$

$$V = \frac{1}{4} \sqrt{\frac{3}{\pi}} \frac{\sqrt{K}}{x} \frac{\eta_2 \left(1 - \frac{1}{4} \eta_2^2\right)}{\left(1 + \frac{1}{4} \eta_2^2\right)^2} \tag{40}$$

where K is kinematic momentum flux (constant), ϵ is virtual kinematic viscosity (constant), and .

$$\eta_2 = \frac{1}{4}\sqrt{\frac{3}{\pi}} \, \frac{\sqrt{K}}{\epsilon} \frac{y}{x}$$

For this case, Reichardt determined the empirical constant $\sqrt{K}/\epsilon$ to be 62.1. Equation (39) is identical with equation (19) with ν replaced by ϵ.

Corrsin (ref. 19) reports experimental transverse velocity profiles through region I for a 3-inch (7.62-cm) diameter heated jet and a 1-inch (2.54-cm) diameter heated jet. Distributions were given for values of x/D of 2, 4, and 6 for the 3-inch (7.62-cm) jet and a value of x/D of 5 for the 1-inch (2.54-cm) jet. In region I, the velocity in the potential core remains constant at $U_m = U_0$ and falls off in the transverse direction exterior to the potential core (see fig. 2). In order to compare these experimental velocity distributions with those of Tollmien and Görtler, it was necessary to translate the jet centerline to the border of the potential core at the respective values of x/D, determine the value of $y_{1/2}$ (where $U = U_m/2$) for each of the distributions, and then calculate the abscissa $y/y_{1/2}$ for selected values of U/U_m for each of the distributions considered. Figure 5 shows the comparison of the experimental distributions of reference 19 with the Tollmien and Görtler distributions. The good agreement in figure 5 indicates that the theories of Tollmien and Görtler are satisfactory for use in predicting the velocity profiles in region I of the jet even though these theories were developed for region II.

(a) Distance from nozzle in axial direction, x = 2D; nozzle diameter, D = 3 inches (7.62 cm).

(b) Distance from nozzle in axial direction, x = 4D; nozzle diameter, D = 3 inches (7.62 cm).

(c) Distance from nozzle in axial direction, x = 6D; nozzle diameter, D = 3 inches (7.62 cm).

(d) Distance from nozzle in axial direction, x = 5D; nozzle diameter, D = 1 inch (2.54 cm).
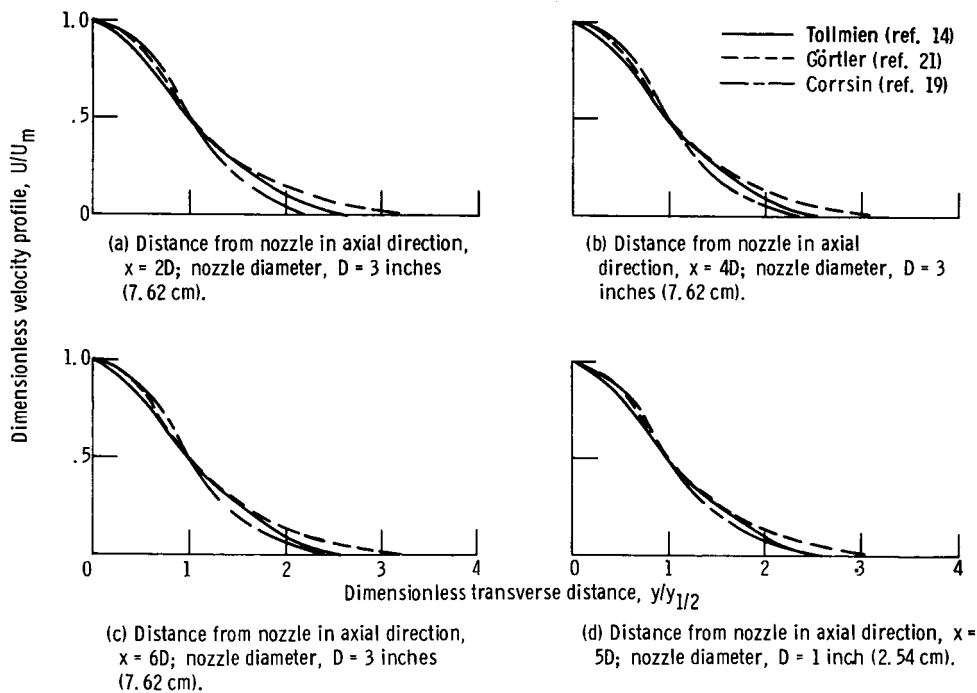
Figure 5. - Velocity profiles in circular turbulent jets.

Under the assumption used in the analyses previously discussed, the transverse velocity distributions differ only by a scale factor. At all sections beyond the tip of the potential core, the velocity distribution is continuous across the line of symmetry, and the ratio σ/x is therefore indicative of the rate of outward spread of the jet. By the same procedure as that explained for the region of flow establishment (region I), reference 13 shows that

$$\frac{U}{U_0} = \sqrt{\frac{1}{\sqrt{\pi}\,K_1}\frac{B_0}{x}}\,\exp\left(-\frac{1}{2K_1^2}\frac{y^2}{x^2}\right) \tag{41}$$

for the two-dimensional jet, and

$$\frac{U}{U_0} = \frac{1}{2K_2}\frac{D}{x}\,\exp\left(-\frac{1}{2K_2^2}\frac{y^2}{x^2}\right) \tag{42}$$

for the circular jet. Equations (41) and (42) show good agreement with experimental data for developed turbulent flow. Equations (41) and (42) were obtained by assuming the same experimental constant σ/x applied to both regions I and II. In addition, they were obtained by use of equation (8), a curve fit of experimental data, rather than from the governing equations considered by Tollmien and Görtler.

Figure 6(a), taken from reference 11, compares experimental data compiled by Förthmann (ref. 23) with the Tollmien and Görtler solutions for a two-dimensional jet and region II. Figure 6(b), also taken from reference 11, compares experimental data compiled by Reichardt (ref. 22) with the Tollmien and Görtler solutions for a circular jet and region II. These curves are plotted with U/U_m as a function of $y/y_{1/2}$; the conversion of Tollmien's solution to this type of plot was discussed previously. The experimental data agree better with Görtler's solution over most of region II, except farther away from the center of the jet, for $y/y_{1/2} > 1.5$.

Reference 1 also presents a plot of experimental data together with the theoretical curves derived by Görtler, namely,

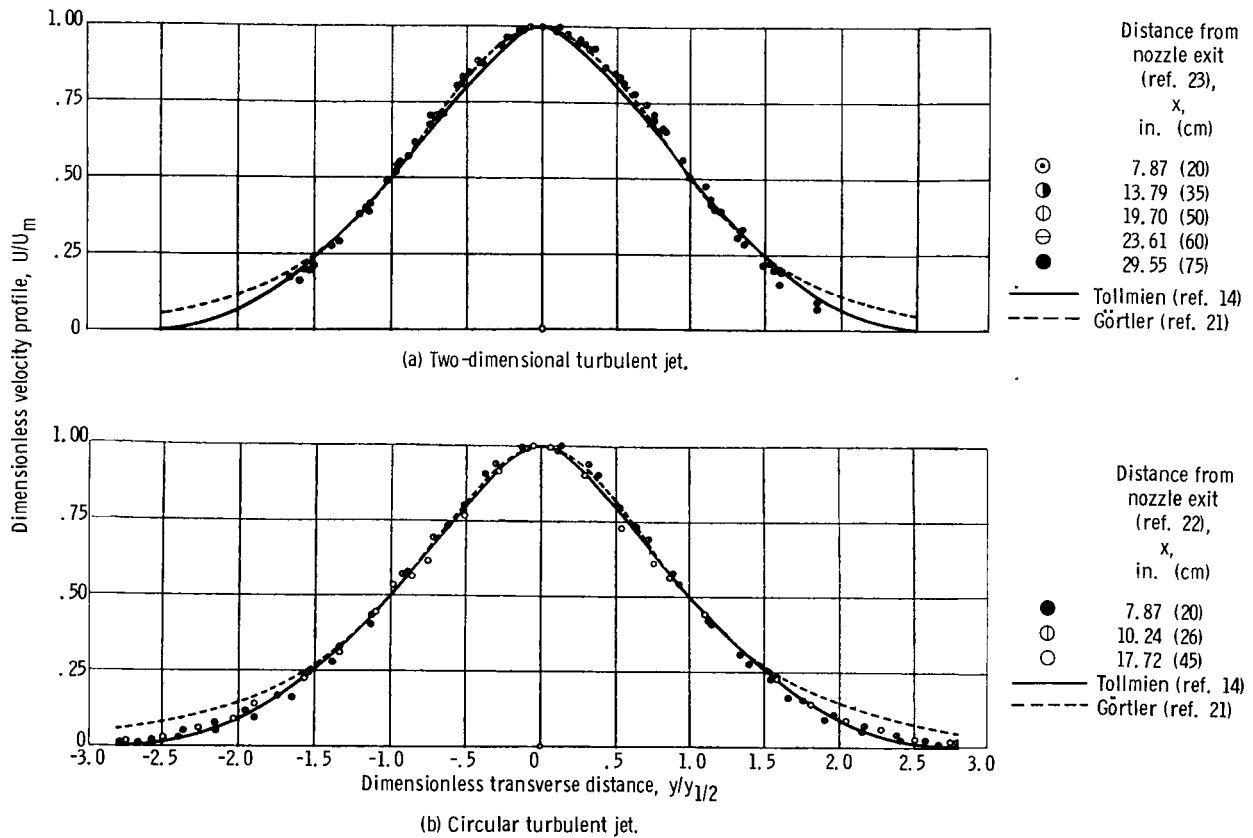$$\frac{U}{U_m} = \frac{1}{\left[1 + \left(7.48\,\frac{y}{x}\right)^2\right]^2} \tag{43}$$

20

Figure 6. - Velocity distribution in two-dimensional and circular turbulent jets. (From ref. 11).

and an error curve

$$\frac{U}{U_m} = \exp\left(-100\,\frac{y^2}{x^2}\right) \tag{44}$$

for the transverse velocity distribution in the region of established flow for a circular jet. The measured transverse velocity distribution is well approximated by either Görtler's solution (eq. (43)) or the error curve (eq. (44)).

In van der Hegge Zijnen (ref. 16), slot jet data are compared against the error curve of equation (44) except that the constant is 70.7 instead of 100. Good agreement is achieved.

Turbulence Distribution Along Centerline

Corrsin (ref. 19) measured the turbulent velocities U'/U_o for a 1-inch (2.54-cm) diameter heated jet at various distances from the nozzle. A plot of these values along the centerline in region II resulted in a straight line, on log-log paper, with slope equal to -0.88 and intercept at 0.84; that is, the equation of the line may be written as

$$\frac{U'}{U_o} = 0.84 \left(\frac{x}{D}\right)^{-0.88} \tag{45}$$

An experimentally determined value of U'/U_o at a value of $x/D = 5$ (region I) obtained in reference 19 does not fall on the extension of this line; hence, it appears that in region I the relation of equation (45) does not apply.

Figure 7 shows a normalized turbulence distribution along the centerline for a circular and a slot jet obtained from references 19 and 20, respectively. Reference 19 shows a plot of U_m/U_o against x/D. By taking the data points for U'/U_o at any x/D and dividing by the value of U_m/U_o at the same value of x/D, a curve of U'/U_m against x/D can be obtained. This plot is shown as the solid curve in figure 7. Also
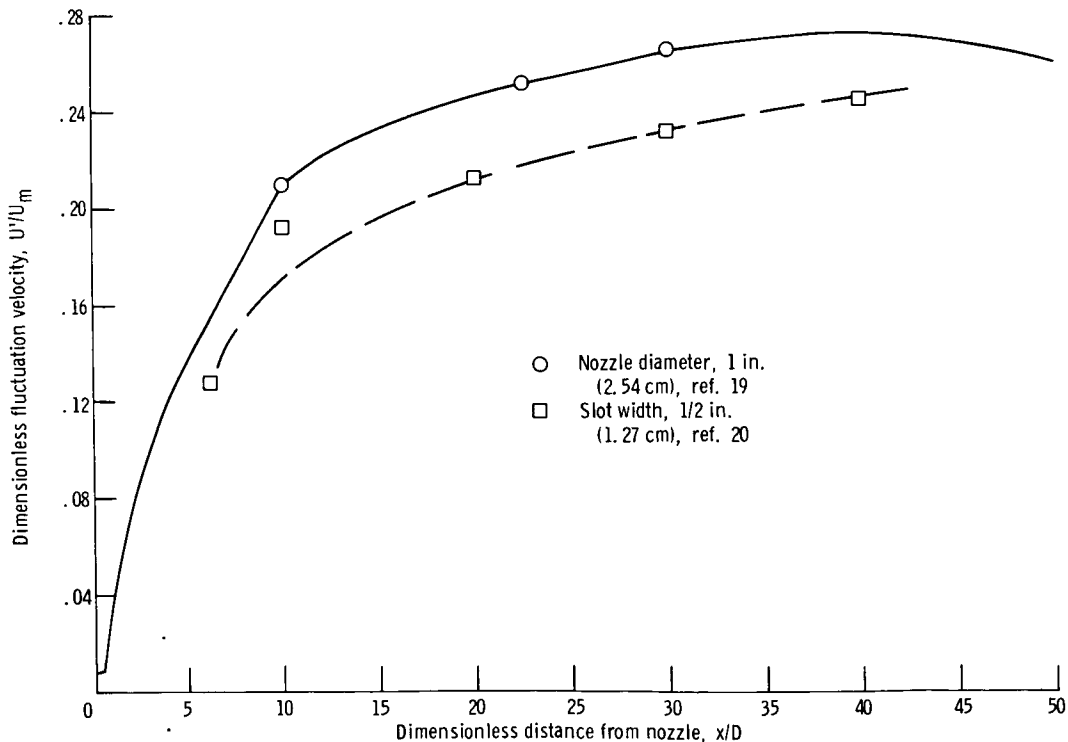

Figure 7. – Turbulence distribution along centerline for a circular and a slot jet.

shown in figure 7 are several experimental values of U'/U_m for a 1/2-inch (1.27-cm) slot jet (ref. 20).

In summary, if the length of the potential core is known, equations (18) and (45) can be combined to give the relation between U'/U_m and x/D in region II.

Pressure Variation Along Jet Centerline

In the analysis of the free jet, ordinarily no variation of static pressure is assumed. By neglecting the turbulent y stress, Tollmien (ref. 14) found the centerline static pressure to be expressible as

$$p_m - p_\lambda = 0.263 K_3^2 \rho U_m^2 \tag{46}$$

where K_3 is an experimental constant expressing the rate of spread of the jet, where the half width of the jet is defined as $\int_0^\infty (U/U_m)^2 \, dy$.

According to Reichardt (ref. 22), $K_3 = 0.075$. Because of the value of K_3, Tollmien concluded that the change in static pressure could be neglected.

Pai (ref. 18) stated that Tollmien's approximation, which assumes no variation in static pressure, could be improved. He obtained

$$p_m - p_\lambda = 0.00165 \rho \, \frac{U_m^2}{2} \tag{47}$$

for the slot jet, and

$$p_m - p_\lambda = -0.00295 \rho \, \frac{U_m^2}{2} \tag{48}$$

for the circular jet. These equations indicate an overpressure in the middle of the jet for the slot jet and an underpressure for the circular jet. However, Townsend (ref. 24) studied the magnitudes of the various terms in the equation solved by Tollmien and concluded that the lateral gradients of the turbulent y stress and static pressure are the dominant terms and that the pressure relation should read

$$p + \rho V'^2 = p_\lambda(x) \tag{49}$$

where $p_\lambda(x)$ is a function of x equal to the static pressure outside the flow. Equation (49) applies for both regions I and II, whereas Tollmien's solution applies only for region II.

The result of Townsend's theoretical study is in direct contradiction to Tollmien's prediction for the centerline static pressure for a slot jet (i.e., eq. (47)). Townsend's result yields an underpressure in the middle of the slot jet. This underpressure has been verified by data of Miller and Comings (ref. 20), which show a dependence of x/B_o. Downstream of $x/B_o = 10$, these data can be represented to within 4 percent by the following equation: .

$$\frac{p_m - p_\lambda}{\rho U_m^2} = -0.0011 \left(\frac{x}{B_o}\right) - 0.016 \tag{50}$$

Reference 16 states the velocity on the jet axis U_m can be obtained from the total pressure head h_m in the jet axis from the relation

$$U_m = f_1 \sqrt{\frac{2h_m}{\rho}} \tag{51}$$

where f_1 is a correction factor for the effect of turbulence. The factor f_1 has been calculated on the assumption that the total pressure head is mainly affected by the axial component of the instantaneous velocity $(U + u)_m$, where u is the velocity fluctuation in the axial direction, so that

$$f_1 = \frac{1}{\sqrt{1 + \left(\frac{U'}{U}\right)_m^2}} \tag{52}$$

where $U' = \sqrt{\overline{u^2}}$. This result has not yet been confirmed by experiment, as far as the authors know.

The peak pressure that existed along the jet centerline in the core region eventually approaches ambient in region II.

Static Pressure Profiles

Static pressure profiles were measured for a slot jet (ref. 20) and are shown in figure 8. The trend in the shape of the curves is toward a stable functional form, varying only in amplitude as the distance from the nozzle increases (see eq. (50)). Reference 20 describes the two lower curves by the relations

$$\left(\frac{p - p_\lambda}{\rho U_m^2}\right)_{x/B_o = 30} = -0.054 \exp\left(-0.3\frac{y^2}{b^2}\right) \tag{53}$$

$$\left(\frac{p - p_\lambda}{\rho U_m^2}\right)_{x/B_o = 40} = -0.060 \exp\left(-0.3\frac{y^2}{b^2}\right) \tag{54}$$
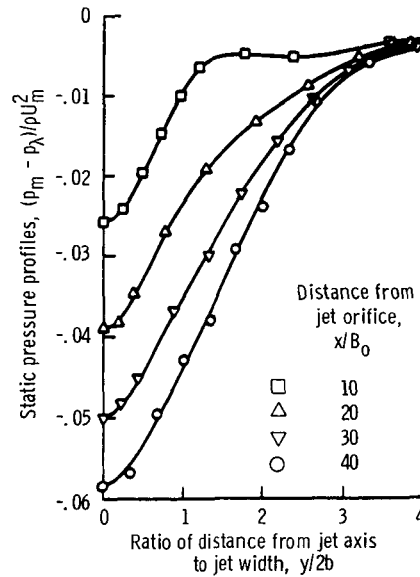

Figure 8. - Static pressure profiles in fully developed region for a slot jet. (From ref. 20.)

Figure 7 of reference 20 shows a plot of the turbulent x-stress profiles in the fully turbulent region. Miller and Comings state that the numerical centerline values on

this figure are nearly equal to the empirical constants in equations (53) and (54). These equations indicate that a static pressure field which is lower than ambient exists throughout the turbulent region of the two-dimensional free jet.

Spread of Free Jet

The spread of the free jet can be determined as soon as the velocity profile as a function of x and y in region II is known. Different experimenters have investigated the spread of the jet. For example, Förthmann (ref. 23) examined the spread of the jet where $y = y_{1/2}$ and obtained a rate of spread of U/U_m equal to 0.097.

If the dimensionless velocity profile behaves as $\exp(-70.7\, y^2/x^2)$, as shown in reference 16, the rate of spreading of $U/U_m = 0.5$ will be 0.0979, compared with Förthmann's value of 0.097. Reference 12 presents experimental data of Förthmann and others, which show the spreading of a slot jet to be the same as the spreading of a circular jet.

REGION OF DEFLECTION (REGION III)

Velocity Distribution

As the flow approaches the impingement plate, flowing in the axial direction, the velocity decelerates rapidly and the pressure increases. At the stagnation point, the velocity is zero and the pressure is a maximum. If the stagnation point is assumed to be the origin, the flow is then in the negative z direction (see fig. 1). For three-dimensional, axisymmetric frictionless flow, Schlichting (ref. 11) states that the axial component of the velocity may be written

$$U = -2az \tag{55}$$

and the radial component of the velocity as

$$V = ar \tag{56}$$

where a is a constant. When z is replaced by $z_n - x$, equation (55) becomes

$$U = -2a(z_n - x) \tag{57}$$

or

$$\frac{U}{az_n} = -2\left(1 - \frac{x}{z_n}\right) \tag{58}$$

This is the form of the equation found in reference 1 for the axial velocity distribution in the deflection region; reference 1 found that

$$a = 98\sqrt{K} \tag{59}$$

where K is the kinematic momentum flux. Similarly, reference 1 found

$$\frac{V}{az_n} = \frac{r}{z_n} \tag{60}$$

or, since $a = 98\sqrt{K}$,

$$\frac{V}{\sqrt{K}\,z_n} = 98\,\frac{r}{z_n} \tag{61}$$

The preceding analysis was obtained for irrotational flow, which, according to reference 10, precludes immediate application of the theory to the impingement region. A theory was developed in reference 10 for axisymmetric inviscid rotational flow. A stream function which automatically satisfied the continuity equation was inserted into the momentum equation (with the pressure term eliminated). Axial and radial velocities were found to be

$$\frac{U}{aL} = -f + \frac{1}{4}r^2 (f'' - b_2) - \frac{1}{8}r^4 \left(K_4 f + \frac{1}{8}f''''\right) + \ldots \tag{62}$$

$$\frac{V}{aL} = \frac{r}{2}\left[f' - \frac{1}{8}r^2 f''' + \frac{1}{24}r^4 \left(K_4 f' + \frac{1}{8}f'''''\right) + \ldots\right] \tag{63}$$

where L is the jet radius at a fixed distance from the nozzle, $-f$ represents the axial velocity along the jet centerline, and primes denote differentiation with respect to z; the jet centerline velocity is approximated by

27

$$f(z) = b_1 z + \frac{1}{2!} b_2 z^2 + \frac{1}{3!} b_3 z^3 + \ldots + \frac{1}{6!} b_6 z^6 \tag{64}$$

where b_1 to b_6 and K_4 are constants. From conditions applied in the analysis, $b_1 = 1$ and $b_4 = 0$. Values of b_2, b_3, b_5, and b_6 are evaluated so that the polynomial $f(z)$ agrees with measured centerline velocities for small values of z, where inviscid flow holds. The constant K_4 is determined such that the value of U observed at some distance from the plate is expressed by the first three terms of equation (62). The radial velocity along the plate can then be expressed as

$$\frac{V(r)}{aL} = \frac{r}{2} \left[1 - \frac{1}{8} b_3 r^2 + \frac{1}{24} \left(K_4 + \frac{1}{8} b_5 \right) r^4 \right] \tag{65}$$

It is shown in reference 10 that the surface velocity computed by equation (65) shows good agreement with the experimental data.

Pressure Distribution

Denoting p' as the total pressure on the jet centerline and p as the static pressure at any arbitrary point, reference 11 states that

$$p' - p = \frac{\rho}{2} (V^2 + U^2) = \rho \frac{a^2}{2} (r^2 + 4z^2) \tag{66}$$

Because this equation was derived for frictionless or irrotational flow, the value of p' is constant along the impingement plate and equals p'_s. Equation (66) may be rewritten as

$$\frac{p'_s}{\rho g} - \frac{p}{\rho g} = \frac{a^2}{2g} (r^2 + 4z^2) \tag{67}$$

At the plate, $z = 0$, so the equation now becomes

$$h'_s - h = \frac{a^2 z_n^2}{2g} \left(\frac{r}{z_n} \right)^2 \tag{68}$$

Reference 1 found that $a = 98\sqrt{K}$ with $K = M/\rho$. Therefore, equation (68) may now be written as

$$\frac{h}{z_n^2} = \frac{h_s'}{z_n^2} - \frac{4800\,M}{\rho g}\left(\frac{r}{z_n}\right)^2 \qquad (69)$$

From plots of the pressure and velocity distributions in reference 1, it was concluded that the stagnation zone could be defined to be interior to a hemisphere with the center at the stagnation point and with a radius of $0.05\,z_n$ (i.e., $r/z_n < 0.05$ and $z/z_n < 0.05$). The effect of diffusion is important beyond these limits. On the boundary of this hemisphere, the pressure intensity deviates from the parabolic shape resulting from equation (69) and approaches the ambient static pressure with increasing r/z_n. The region of established radial flow starts where the pressure gradient is nearly zero (i.e., $r/z_n > 0.3$ (ref. 1)).

Experimental data obtained for a circular jet are presented in reference 10. The pressure difference along the impingement plate $(p_r)_{z=0} - p_\lambda$ was made dimensionless by use of the nozzle dynamic pressure $\rho U_0^2/2$. The pressure fell from a maximum value p_s' at the stagnation point to p_λ (ambient) at a radius of 1.6 to 3 nozzle diameters; hence, the region of impingement, which was quite small, was found to extend from 1.6 to 2.2 diameters axially and 1.6 to 3 diameters radially, with the stagnation point at the center.

Velocity profiles were obtained at various radial stations and indicated that maximum values existed near the surface. Plots of these maximum velocities and of those computed from the measured pressure distribution (assuming no dissipation in the flow $\left(\text{i.e., } p_s' - (p_r)_{z=0} = \frac{1}{2}\rho V_m^2\right)$ showed that the measured and computed values coincided up to 0.6 to 1.2 diameters for nozzle to plate spacings of 4 to 12 diameters, respectively. Hence, it appears that the effect of viscous dissipation is negligible up to these distances, which, according to reference 10, are about 40 percent of the radial extent of the deflection region.

WALL JET REGION (REGION IV)

Velocity Decay Along Plate

In analyzing the so-called wall jet region (region IV, fig. 1), Glauert (ref. 25) divided the flow region into two parts: (1) an inner layer where the effect of the wall is present, and (2) an outer layer which is characterized by the features of a free turbulent flow. The velocity at the boundary between these two layers is the maximum velocity. It has been shown (refs. 26 to 28) that this maximum velocity may be expressed by the relation

$$V_m = \frac{\text{Constant}}{r^n} \tag{70}$$

Four different values of n (1.14, 1.1, 1.143, and 1.12) have been found by each of four different investigators (refs. 25 to 28). Glauert (ref. 25) was the first, however, to formulate equation (70) using n = 1.14, which gives results very close to experimental values. In equation (70) the power of r is greater than 1 for a radial wall jet, whereas for a free jet it is equal to 1; hence, the decay of the maximum velocity along the plate is faster than that of a free jet.

Velocity Profile Through Wall Jet

Glauert obtained solutions for the two layers of flow mentioned previously. For the inner layer, he assumed the 1/7 power velocity profile; for the outer layer, he assumed that the eddy viscosity was constant. The solutions were then matched at the boundary between the two layers, where the shear stress was assumed to be zero. The result was a velocity distribution throughout the jet, dependent on a single constant α. Since α varies with Reynolds number, the velocity profiles vary with distance. However, the variation in α is very small, and so the velocity field is approximately similar.

Other investigators (refs. 1 and 12) found it useful to employ a reference boundary velocity V_{RB} where

$$V_{RB} = \frac{\text{Constant}}{r} \tag{71}$$

The reference velocity V_{RB} is the centerline velocity at r of a hypothetical free jet issuing radially from the stagnation point and can be obtained by extrapolating the velocity profile of the outer jet region to the wall (see fig. 1). Görtler's free-jet solution for the outer layer was discussed earlier and can be used as follows:

$$\frac{V}{V_{RB}} = 1 - \tanh^2 K_5 \frac{z}{r} \tag{72}$$

where K_5 is an integration constant.

Abramovich (ref. 12) used the relation

$$\frac{V}{V_m} = (1 - \zeta^{3/2})^2 \tag{73}$$

to represent the velocity distribution through the outer layer of the wall jet; here,

$$\zeta = \frac{z - \delta}{b'} \tag{74}$$

Figure 9 shows a plot of V/V_m against $z/z_{1/2}$ for the theories of Glauert, Abramovich, and Görtler. To obtain the curve for Görtler's distribution as shown on figure 9, equation (72) was multiplied by V_{RB}/V_m. If $K_5 = 10$ (ref. 1) and $r = (z_{1/2} K_5/K_6)$, then V_{RB}/V_m, and K_6 can be calculated by using the boundary conditions $V/V_m = 1/2$ at $z/z_{1/2} = 1$ and $V/V_m = 1$ at $z/z_{1/2} = 0.2$ (ref. 25). The three curves in figure 9 show fairly good agreement.
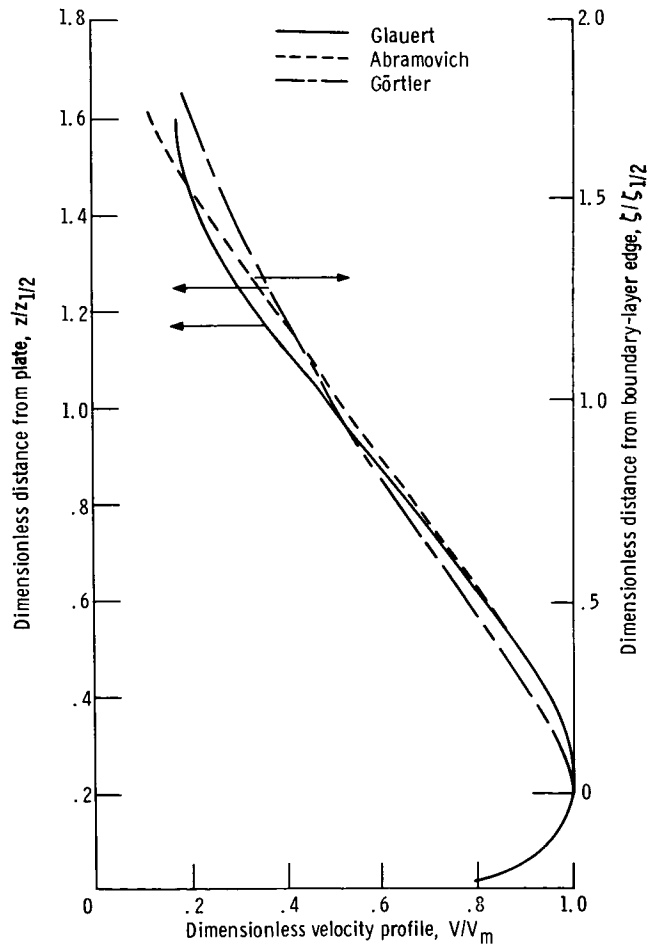

Figure 9. - Comparison of wall-jet theoretical velocity profiles.

Reference 1 reports experimental data for the velocity distribution through the wall jet. If a value of $K_5 = 10$ is used in equation (72), good agreement with the data is obtained. This is shown in figure 10. Here, in the outer zone, the experimental data can be approximated almost equally well by

$$\frac{V}{V_{RB}} = 1 - \tanh^2 10 \frac{z}{r} \qquad z > \delta \tag{75}$$

or by the error curve

$$\frac{V}{V_{RB}} = \exp\left(-100 \frac{z^2}{r^2}\right) \tag{76}$$

Bakke (ref. 28) showed by means of experimental data that the velocity gradient near the wall is much greater than that of Glauert's analysis (ref. 25). Figure 11 shows a
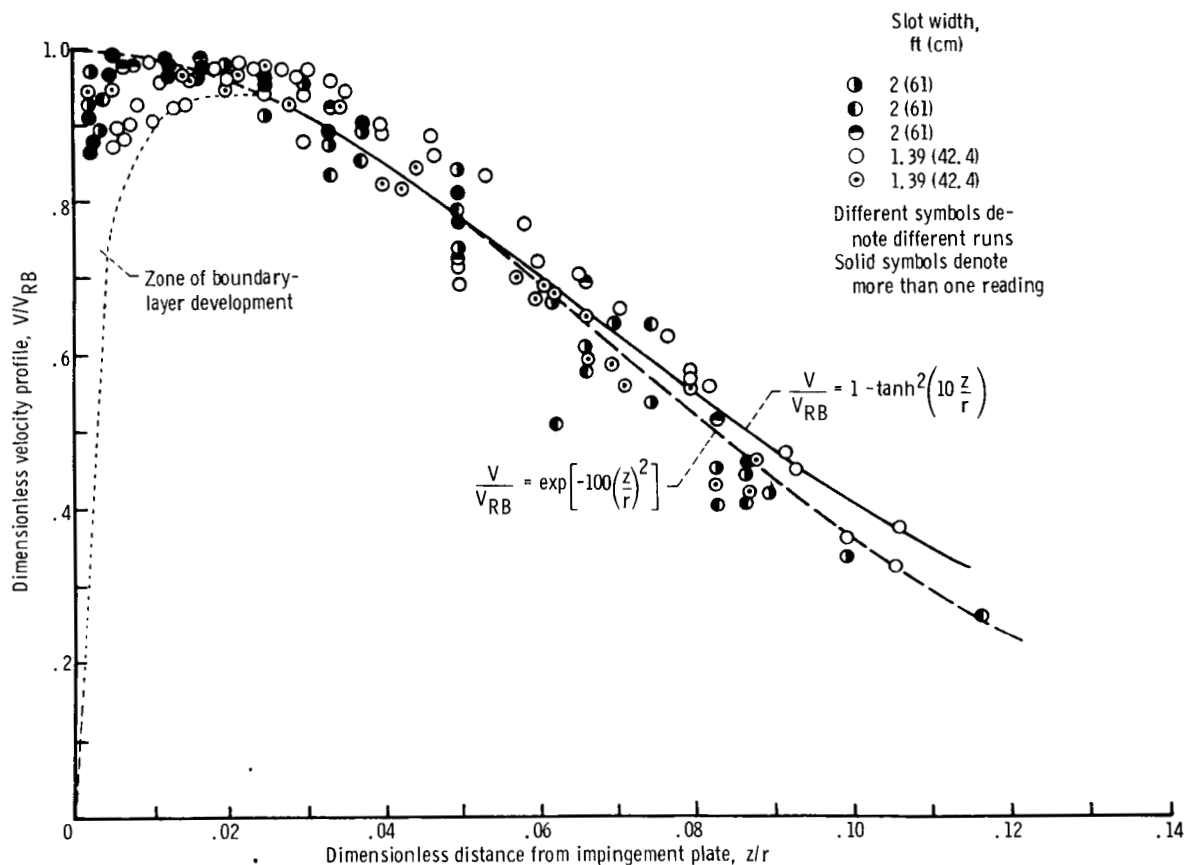

Figure 10. – Velocity distribution in region of radial flow (region IV). (From ref. 1.)
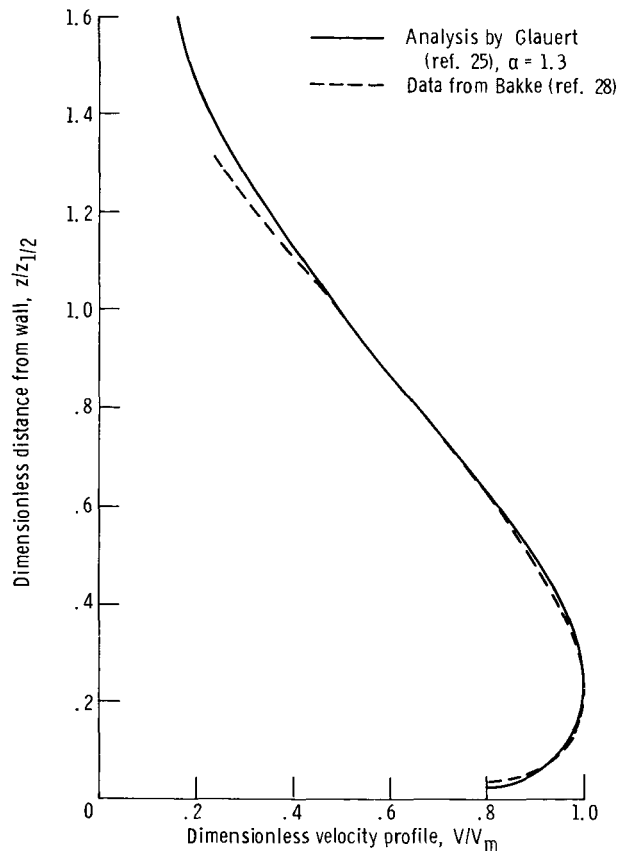
32

Figure 11. - Comparison of velocity profiles of wall jet by
Glauert and Bakke.

comparison between Bakke's data and Glauert's analysis; it can be seen that, except for the profile in the boundary layer near the plate, the similarity law is well satisfied.

As experimentally determined by Bradshaw and Gee (ref. 29), Schwarz and Cosart (ref. 30), and Kruka and Eskinazi (ref. 31) the turbulent shear stress was zero not at $z = \delta$, but rather at a point closer to the wall. Also, several investigators (refs. 26, 29, and 32 to 34) have reported that the turbulence effects were found to be considerably higher than those corresponding to a flat plate. These turbulence effects probably contributed to producing a velocity profile near the wall whose power slope was measured as 1/11 to 1/14.

Spalding (ref. 35) found a method where no knowledge of the shear stress at $z = \delta$ is required, and McGahan (ref. 36) showed that this method and the two-layer method with shear stress zero at $z = \delta$ give essentially similar results.

More recently, Cadek (ref. 37) analyzed the behavior of two-dimensional impinging jets, based on the assumptions of normal impingement, a flat, constant temperature impingement surface, incompressible flow and constant fluid properties, and wall temperature higher than jet temperature.

The impingement region treatment includes Cadek's own static pressure measurements; integral methods are applied to the calculation of the inner flow associated with the wall-boundary layer. The outer layer is assumed to behave as a free jet.

The analysis is based on integral methods appropriate for the laminar flow near the stagnation region. An approach using the boundary-layer thickness at the position where the velocity within the boundary layer has been reduced to just 50 percent of the maximum velocity in the boundary layer has allowed Cadek to eliminate the effect of the distance from the jet orifice x/B_o.

In summary, the integral approach using the two-layer model, despite its inconsistencies, provides a generally good means of predicting velocity profiles. Additional investigations are in order to obtain more information about the power slope of the profile near the wall, assumed as 1/7 for theory and obtained as 1/11 to 1/14 for data.

Spread of Wall Jet

The spreading of the wall jet in terms of the half value $z_{1/2}$ can be predicted by use of the equation

$$\frac{z_{1/2}}{D} = \text{Constant} \left(\frac{r}{D}\right)^m \tag{77}$$

The values of the exponent m were found in references 26 to 28 to be 0.9, 1.028, and 0.94, respectively.

The spread of the wall jet, as in the spread of the free jet, can be determined as soon as the velocity profile as a function of r and z is known. If the dimensionless velocity profile behaves as given in equation (76), the rate of spreading with respect to r of the half width of the wall jet (where $V/V_m = 0.5$) will be 0.083. Experimental data in figure 7 of Poreh et al. (ref. 26) show the rate of spreading of the wall jet to be approximately 0.09.

POSSIBLE APPLICATIONS FOR USE IN HEAT-TRANSFER CORRELATIONS

The ultimate objective of the impingement cooling program was the determination of heat-transfer correlations adequate for design purposes. Although this report is restricted to a study of the flow characteristics of an impinging jet, it seems in order to make a few remarks relative to what information may be useful in obtaining the desired heat-transfer correlations.

34

Since the centerline jet velocity is constant in the potential core and decreases beyond the apex of this core, maximum heat transfer will be obtained if the impingement plate is separated from the nozzle exit by the length of the potential core. If this length is not known, an assumed value of about 6.1 nozzle diameters may be used. In determining the heat transfer at the stagnation point, the use of the arrival velocity in evaluating the Reynolds number has proved useful (refs. 6 and 7). The arrival velocity is that velocity which would exist at the same distance from the nozzle as the stagnation point if no impingement plate were present.

If the plate lies inside the potential core, the arrival velocity is equal to the nozzle exit velocity since the velocity within the potential core is constant. If the impingement plate lies outside the potential core, the arrival velocity may be calculated from equation (18)

$$\frac{U_m}{U_o} = \frac{C_2}{\frac{x}{D}} \qquad (18)$$

where x is replaced by z_n, and U_m then becomes the arrival velocity.

Similarly, the velocity fluctuations due to turbulence may be calculated from equation (45)

$$\frac{U'}{U_o} = 0.84 \left(\frac{x}{D}\right)^{-0.88} \qquad (45)$$

A combination of equations (45) and (18) permits calculation of U' in terms of U_m, as previously illustrated in figure 7. If heat-transfer data do not correlate on the arrival velocity, this velocity may be corrected by use of the fluctuation velocity, and another attempt at correlation may be made.

To supply adequate impingement cooling, the proper spacing of free-jet nozzles must be known. This nozzle spacing is dictated by the rate at which the jet spreads. Abramovich (ref. 12) reported a value of $d(y_{1/2})/dx = 0.097$.

Since the primary interest in the impingement flow investigation is the determination of heat transfer, some remarks relative to heat transfer at the stagnation point are in order. In order to estimate the heat transfer at the stagnation point of an impinging flow, the local radial velocity gradient $(dV_m/dr)_{r=0}$, which appears as a parameter in the usual stagnation-point heat-transfer equation, must be evaluated. This can be done experimentally by relating this parameter to the static pressure distribution on the surface in the immediate neighborhood of the stagnation point. Assuming incompressible

flow, this parameter is proportional to the square root of the curvature of the pressure distribution at the stagnation point and can be obtained from experimental data from the equation

$$\left(\frac{dV_m}{dr}\right)_{r=0} = \sqrt{\frac{2R}{r_w^2}} \sqrt{\frac{T_s}{\left(\frac{r}{r_w}\right)^2}\left(1 - \frac{p}{p_s'}\right)}$$

where

r_w wetted radius of impingement surface

T_s stagnation point temperature of fluid

R gas constant

p_s' total pressure at stagnation point

This parameter can be calculated as follows: to determine this parameter, pressure data in the form $1 - (p/p_s')$ are first plotted as a function of $(r/r_w)^2$. The slope of the resulting curve is determined graphically at $r = 0$, and the value of $(dV_m/dr)_{r=0}$ is then computed from the preceding equation.

At distances along the plate from the stagnation point, it has been shown that a maximum velocity exists at the boundary between an inner flow layer, where wall effects are felt, and an outer layer, which is characterized by the features of a free jet. This velocity is expressed by equation (70)

$$V_m = \frac{\text{Constant}}{r^n} \tag{70}$$

for which values of n ranging from 1.1 to 1.143 have been reported.

If heat-transfer data in the wall-jet region cannot be correlated by use of the maximum radial velocity, other radial velocities must be used. Three methods for predicting the velocity profile through the wall jet have been discussed.

Although the present review was restricted to single jets impinging on a flat plate, the information presented may be applied to the use of multiple jets. Since the spread of the jet is discussed, this information may be applicable for locating other jets in an array so that maximum heat-transfer coefficients could be achieved along a surface. In this way, for example, it may be possible to use rows of jets to obtain maximum cooling along the suction and pressure surfaces of turbine vanes or blades.

36

There is some evidence (ref. 38) that heat transfer from impinging jets on flat plates and on curved surfaces is similar. With additional flow studies of jets impinging on curved surfaces to verify similar flow characteristics, the discussions presented herein may eventually be applicable to such surfaces as turbine vane or blade leading edge regions. Another investigator who has studied heat transfer from the inner side of concave surfaces is D. E. Metzger (ref. 39). This study is directly applicable to impingement cooling of vane or blade leading edges.

CONCLUDING REMARKS

An extensive survey of the flow characteristics of a single jet impinging on a flat surface led to the following conclusions:

1. The flow field can be divided into four distinct regions. Methods for predicting velocities and pressures in the various regions agree reasonably well with experimental data.

2. Additional work is required to determine the influence of flow Reynolds number on core length and the large discrepancy between the theoretical and experimental velocity gradients near the wall.

3. The length of the potential core was found experimentally to vary from about 4.7 to about 7.7 nozzle diameters by different investigators. This length has also been shown theoretically to equal 3/32 times the nozzle exit Reynolds number for a laminar jet and to be independent of nozzle exit Reynolds number for a fully developed turbulent jet. By combining Tollmien's analysis for a fully developed turbulent jet with an experimental value for the spreading of the half width of the jet, the potential core length was found to be about 6.1 nozzle diameters.

4. The spreading of a free jet where the velocity equals one-half the maximum velocity was found to be 0.097 times the distance from the jet nozzle.

5. The axial velocity for a free jet is constant and equal to the nozzle exit velocity over a distance equal to the potential core length.

6. The axial velocity downstream of the potential core for a circular free jet is inversely proportional to the distance from the jet nozzle expressed in nozzle diameters. For a slot jet, the axial velocity downstream of the potential core is inversely proportional to the square root of the distance from the jet nozzle in slot widths. The constants of proportionality are the potential core length for the circular jet and the square root of the potential core length for the slot jet, respectively. Impinging jets behave like free jets up to several nozzle diameters from the surface.

7. An equation for determining velocity profiles normal to the jet axis through the potential core is available; it depends on a single experimental constant, namely, the length of the potential core. This equation was developed by Albertson.

8. Velocity profiles beyond the potential core region can be determined from the anasyses of Görtler and Tollmien. Equations for these profiles depend on a single empirical constant. Good agreement with experimental data has been achieved.

9. Equations are available for calculating turbulence velocity fluctuations for the circular jet if the length of the potential core is known. An assumed potential core length of about 6.1 nozzle diameters may be used if the actual length is not known.

10. The radial velocity component in the deflection region is proportional to the radial distance from the stagnation point.

11. Three analytical solutions (those of Abramovich, Glauert, and Görtler) for the velocity profiles through the wall jet region are available.

Lewis Research Center,
    National Aeronautics and Space Administration,
        Cleveland, Ohio, November 5, 1969,
            720-03.

38

APPENDIX - SYMBOLS

A	area of jet cross section	h'	total pressure head, $p'/\rho g$
a	constant		
B	width of potential core	J	total momentum flux
B_o	slot width	K	kinematic momentum flux, J/ρ
b	half width of free jet		
b'	distance from edge of boundary layer to edge of wall jet	$K_1, \ldots, K_6$	constants
		L	jet radius at fixed distance from nozzle
$b_1, \ldots, b_6$	constants in polynomial approximation for velocity along jet centerline	l, l_1	mixing lengths
		M	mass
		m, n	exponents
C_1	dimensionless potential nominal core length for slot jet	p	static pressure
		p'	total pressure
C_2	dimensionless potential nominal core length for circular jet	Q	volumetric flow rate
		R	gas constant
c	constant	Re_o	Reynolds number based on either nozzle diameter or slot width
D	nozzle diameter		
E	energy flux	r	distance from stagnation point in radial direction
f	polynominal approximation for velocity along jet centerline	s	fixed distance from nozzle
		T_s	stagnation point temperature
f_1	turbulence correction factor		
		t	time
$f', \ldots, f'''''$	derivatives of f with with respect to z	U	velocity in axial direction
		U'	time mean of square of instantaneous velocity fluctuation, $\sqrt{\overline{u^2}}$
g	acceleration due to gravity		
h	pressure head, $p/\rho g$	u	instantaneous axial velocity fluctuation

V	velocity in radial direction	η_2	$\frac{1}{4}\sqrt{\frac{3}{\pi}}\frac{\sqrt{K}}{\epsilon}\frac{y}{x}$
V'	time mean of instantaneous radial velocity fluctuation		
V_{RB}	reference velocity	λ	$\frac{1}{2}\sqrt{\frac{U_{m,s}s}{\epsilon_s}}$
v	instantaneous radial velocity fluctuation	ν	laminar flow kinematic viscosity
x	distance from nozzle in axial direction		
x_c	absolute potential core length	ξ	$\sqrt{\frac{3K}{16\pi}\frac{y}{\nu x}}$
		ρ	density
y	distance from centerline in radial direction	σ	standard or root-mean-square deviation
$y_{1/2}$	value of y for which $U = 1/2\ U_m$	τ	turbulent shearing stress
z	distance from impingement plate in axial direction	φ	$\frac{y}{ax}$
		χ_1	empirical constant

Subscripts:

z_n	distance between nozzle and impingement plate	m	centerline or maximum
		max	maximum
$z_{1/2}$	value of z for which $V = 1/2\ V_m$	min	minimum
α	constant	o	average nozzle exit
γ	proportionality constant	r	radial position
δ	boundary-layer thickness	s	stagnation point value or fixed distance from nozzle
ϵ	virtual kinematic viscosity		
ζ	$\frac{z-\delta}{b}$	sc	settling chamber
		w	wetted
η_1	$\frac{\lambda y}{x}$	λ	ambient

REFERENCES

1. Poreh, Michael; and Cermak, J. E.: Flow Characteristics of a Circular Submerged Jet Impinging Normally on a Smooth Boundary. Sixth Midwestern Conference on Fluid Mechanics. Univ. Texas, 1959, pp. 198-212.

2. Kim, Tong Soo: Analysis of Flow Characteristics in Circular, Submerged, Impinging Jets. Ph. D. Thesis, Illinois Inst. Tech., 1967.

3. Vickers, J. M. F.: Heat Transfer Coefficients Between Fluid Jets and Normal Surfaces. Ind. Eng. Chem., vol. 51, no. 8, Aug. 1959, pp. 967-972.

4. McNaughton, K. J.; and Sinclair, C. G.: Submerged Jets in Short Cylindrical Flow Vessels. J. Fluid Mech., vol. 25, pt. 2, June 1966, pp. 367-375.

5. Cederwell, K.: The Initial Mixing on Jet Disposal into a Recipient. Publ. Nos. 14 and 15, Div. of Hydraulics, Chalmers Univ. of Technology, Göteborg, Sweden, 1963.

6. Gardon, Robert; and Cobonpue, John: Heat Transfer Between a Flat Plate and Jets of Air Impinging on It. International Developments in Heat Transfer. ASME, 1963, pp. 454-460.

7. Chamberlain, John E.: Heat Transfer Between a Turbulent Round Jet and a Segmented Flat Plate Perpendicular to It. M. S. Thesis, Newark College of Engineering, 1966.

8. Gardon, Robert; and Akfirat, J. Cahit: Heat Transfer Characteristics of Impinging Two-Dimensional Air Jets. J. Heat Transfer, vol. 88, no. 1, Feb. 1966, pp. 101-108.

9. Levey, Harris C.: The Back Effect of a Wall on a Jet. geit. f. Angew. Math. Phys., vol. 11, no. 2, 1960, pp. 152-157.

10. Tani, I.; and Komatsu, Y.: Impingement of a Round Jet on a Flat Surface. Procedings of the Eleventh International Congress of Applied Mechanics. Henry Görtler, ed., Springer-Verlag, 1966, pp. 672-676.

11. Schlichting, Hermann (J. Kestin, trans.): Boundary-Layer Theory. Sixth ed., McGraw-Hill Book Co., Inc., 1968.

12. Abramovich, Genrikh N.: The Theory of Turbulent Jets. MIT Press, 1963.

13. Albertson, M. L.; Dai, Y. B.; Jensen, R. A.; and Rouse, Hunter: Diffusion of Submerged Jets. ASCE Trans., vol. 115, 1950, pp. 639-697.

14. Tollmien, Walter: Calculation of Turbulent Expansion Processes. NACA TM 1085, 1945.

15. Schauer, J. J.; and Eustis, R. H.: The Flow Development and Heat Transfer Characteristics of Plane Turbulent Impinging Jets. Tech. Rep. 3, Dept. Mech. Eng., Stanford Univ. Sept. 30, 1963.

16. Hegge Zijnen, B. G. van der: Measurements of the Velocity Distribution in a Plane Turbulent Jet of Air. Appl. Sci. Res., vol. 7, sec. A, 1957-1958, pp. 256-276.

17. Trentacoste, Nicholas; and Sforza, Pasquale M.: An Experimental Investigation of Three-Dimensional Free Mixing in Incompressible, Turbulent, Free Jets. Rep. PIBAL-871, Polytechnic Inst. of Brooklyn (AFOSR-66-6651, DDC No. AD-634254), Mar. 1966.

18. Pai, Shi-i: Fluid Dynamics of Jets. D. Van Nostrand, Co., Inc., 1954.

19. Corrsin, Stanley: Investigation of Flow in an Axially Symmetrical Heated Jet of Air. NACA Wartime Report W-94, 1943.

20. Miller, David R.; and Comings, Edward W.: Static Pressure Distribution in the Free Turbulent Jet. Fluid Mech., vol. 3, pt. 1, Oct. 1957, pp. 1-16.

21. Görtler, H.: Berechnung von Augfaben der freien Turbulenz auf Frund eines neuen Naherungsansatzes. Zeit. f. Angew. Math. Mech., vol. 22, no. 5, Oct. 1942, pp. 240-254.

22. Reichardt, H.: Gesetzmässigkeiten der freien Turbulenz. VD1-Forschungsheft, 414, 1942. (2nd ed., 1951.)

23. Förthmann, E.: Turbulent Jet Expansion. NACA TM 789, 1936.

24. Townsend, A. A.: The Structure of Turbulent Shear Flow. Cambridge Univ. Press, 1956.

25. Glauert, M. B.: The Wall Jet. J. Fluid Mech., vol. 1, pt. 6, Dec. 1956, pp. 625-643.

26. Poreh, M.; Tsuei, Y. G.; and Cermak, J. E.: Investigation of a Turbulent Radial Wall Jet. J. Appl. Mech., vol. 34, no. 2, June 1967, pp. 457-463.

27. Brady, W. G.; and Ludwig, G.: Theoretical and Experimental Studies of Impinging Uniform Jets. J. Am. Helicopter Soc., vol. 8, no. 2, Apr. 1963, pp. 1-13.

28. Bakke, P.: An Experimental Investigation of a Wall Jet. J. Fluid Mech., vol. 2, pt. 5, July 1957, pp. 467-472.

29. Bradshaw, P.; and Gee, M. T.: Turbulent Wall Jets with and without an External Stream. ARC R&M-3252. 1962.

30. Schwarz, W. H.; and Cosart, W. P.: The Two-Dimensional Turbulent Wall-Jet. J. Fluid Mech., vol. 10, pt. 4, June 1961, pp. 481-495.

31. Kruka, V.; and Eskinazi, S.: The Wall-Jet in a Moving Stream. J. Fluid Mech., vol. 20, pt. 4, Dec. 1964, pp. 555-579.

32. Myers, G. E.; Schauer, J. J.; and Eustis, R. H.: The Plane Turbulent Wall Jet. Part 2 - Heat Transfer. Tech. Rep. 2, Eng. Dept., Stanford Univ., Dec. 1, 1961.

33. Patel, R. P.: Self-Preserving Two-Dimensional Turbulent Jets and Wall Jets in a Moving Stream. MS Thesis, McGill University, 1962.

34. Sigalla, A.: Measurements of Skin Friction in a Plane Turbulent Wall Jet. J. Roy. Aeron. Soc., vol. 62, no. 576, Dec. 1958, pp. 873-877.

35. Spalding, D. G.: A Unified Theory of Friction, Heat Transfer and Mass Transfer in the Turbulent Boundary Layer and Wall Jet. Rep. ARC-CP-829, Aeronautical Research Council, Great Britain, 1965.

36. McGahan, Wallace A.: Incompressible, Turbulent Wall Jet in an Adverse Pressure Gradient. Rep. 82, Gas Turbine Lab., Massachusetts Inst. Tech., Sept. 1965.

37. Cadek, Frederick F.: A Fundamental Investigation of Jet Impingement Heat Transfer. PhD Thesis, Univ. Cincinnati, 1968.

38. Burggraf, Frederick: Average Heat Transfer Coefficients with a Row of Air Jets Discharging into a Half Cylinder. MS Thesis, Univ. Cincinnati, 1967.

39. Metzger, D. E.; Yamashita, T.; and Jenkins, C. W.: Impingement Cooling of Concave Surfaces with Lines of Circular Air Jets. Paper 68-WA/GT-1, ASME, Dec. 1968.